ENG. Struct. Civ. Eng. 2026, 20(4): 721–735
https://doi.org/10.1007/s11709-026-1292-x

RESEARCH ARTICLE

Self-healing of asphalt concrete under cyclic loading: Experimental and numerical study

Sergei INOZEMTCEV[a], Denis JELAGIN[b*], Evgeniy KOROLEV[c], Tuan Huu LE[a], Hassan FADIL[b], Manfred N. PARTL[b], Feng CHEN[d]

[a] *National Research Moscow State University of Civil Engineering, Moscow 129337, Russia*
[b] *KTH Royal Institute of Technology, Brinellvägen 23, Stockholm 10044, Sweden*
[c] *St. Petersburg State University of Architecture and Civil Engineering, Petersburg 190005, Russia*
[d] *School of Transportation, Southeast University, Nanjing 211189, China*
[*] *Corresponding author. E-mail: denis.jelagin@abe.kth.se*

ABSTRACT The present study aims at experimentally and numerically investigating the effect of an encapsulated healing agent on the mechanical characteristics of a stone mastic asphalt (SMA-15) after cyclic loading. As healing agents a thiol-containing urethane AR-polymer (ARP) and a sunflower oil (SfO) are used. The comparison of self-healing results in asphalts show that the use of encapsulated ARP allows to restore strength and stiffness up to 93% of whereas encapsulated SfO restores up to 90%. Without capsules, the self-healing effect is 81%. After self-healing, the structure of asphalt concrete with encapsulated ARP is capable of withstanding 15% and 22% more loads than original SMA-15 and SMA-15 with encapsulated SfO, respectively. To gain numerical insight into the mechanical behavior of the capsules in SMA-15, micromechanical finite element modeling is employed. The model is used to evaluate the effect of damage formation with respect to stresses and strains in the capsules and their propensity to breakage.

KEYWORDS self-healing, asphalt concrete, capsules, cyclic test, 4-point bending, micromechanics, finite element method

1 Introduction

Binder modifiers, such us polymers, adhesion promoters, stabilizers, etc., are applied to improve the properties of asphalt [1,2] and increase the damage resistance of the material [3–5]. A relatively new approach is the use of modifiers that improve the self-healing potential of asphalt [6–9]. Such modifiers potentially increase the service life of pavements by at least partially healing damage induced by traffic loads [10–13].

Modifiers for promoting self-healing of asphalt concrete are often synthesized in capsules that contain healing agents of various natures [11,14–16]. The use of capsules is clearly different from other healing options where steel fibers or particles are mixed into the asphalt for inducing inductive crack-healing [17]. The healing agents are released after the capsules have been destroyed during crack formation in their vicinity, thus starting the healing process of the asphalt concrete. The effectiveness of the healing process depends on many factors. One of the main factors is the nature of the substance that acts as healing agent. Traditionally, various organic compounds are used, such as oils and rejuvenators [14–16] or polymers [11]. When synthesizing an encapsulated modifier, the choice of healing agent depends on its chemical nature, degree of affinity with bitumen and its ability to form technological mixtures as well as structural bonds during healing [18].

The use of capsules as a container for the healing agent determines the conditions for activating the self-healing process. It was previously proven through mechanical testing, X-Ray Computed Tomography investigations and numerical modeling [19–21] that alginate capsules survive normal service loads applied to asphalt concrete and are destroyed when a crack tip is located close to a capsule, triggering the self-healing process. The

Article history: Received Apr 23, 2025; Accepted Nov 20, 2025

development of cracks in asphalt concrete begins with the formation of microcracks, which subsequently grow and coalesce resulting in macroscale damage [22–25]. It is obvious that the size of the cracks as well as the temperature and loading conditions are important parameters, determining the efficiency of an encapsulated modifier. Currently, researchers use various approaches to assess the self-healing effect with asphalt concrete [26–30], usually employing static loading schemes, inducing relatively large cracks in specimens. This size of cracks is not necessarily suited for optimal healing pavement deterioration, as it may be hypothesized that the healing potential is higher when micro-cracks are induced in asphalt. Accordingly, healing of micro-cracks gradually induced under cyclic loading received attention recently [31–34]. In Ref. [31] the evolution of asphalt modulus under cyclic loading combined with rest periods was investigated and up to 90% recovery of the modulus during the adopted rest periods (4 h) was reported. Cyclic loading on asphalt concrete with steel wool fibers [32] was shown to decrease the healing effect proportional to the number of loading cycles. The simulations in Ref. [33] attempted to quantify the effect of the number of cracks induced in asphalt during multiple cyclic loading on the loss of self-healing efficiency [34]. evaluated characteristics for the release of the healing agent from capsules under cyclic loading, showing that the amount of released agent increased with load cycles. In spite of considerable progress achieved in this field, the performance of asphalts containing self-healing agents, during gradual progression of damage under cyclic loading is not fully understood yet. In particular, methods are lacking for quantifying the effect of damage accumulation on the activation of capsules. Therefore, it is the intention of this study is to address this gap.

This article aims to examine experimentally and numerically the processes of damage accumulation and healing of asphalts modified with an encapsulated healing agent. Capsules with thiol-containing urethane AR-polymer (ARP) and sunflower oil (SfO) were used to modify stone mastic asphalt (SMA). SfO is used as a popular healing agent frequently used in Refs. [35,36]. The ARP has recently been proposed as an alternative healing agent, which instead of softening the bitumen promotes gluing of crack surfaces [11]. Self-healing properties of asphalts were assessed based on the evolution of strength and stiffness of SMA samples during repeated compression as well as 4-point beam bending tests after a 7 d rest period. Furthermore, in order to gain some micro-mechanical insight into the problem, a micro-mechanical finite element (FE) model of asphalt was developed, following the methodology proposed in [37]. In the model, asphalt is represented as a 4-phase material, consisting of mortar, aggregates, air voids and capsules with the healing agent. The model was used to investigate the stress-state in an asphalt beam under 4-point bending (4PB). A simple strain-softening model was proposed to simulate damage formation in the asphalt during the test. To gain insight into capsule breakage, stresses and strains induced in the capsules were examined. Furthermore, the effect of damage in asphalt beam on stresses induced in the capsules was evaluated.

2 Materials and methods

2.1 Materials

The study was performed on SMA with a bitumen content of 7% with penetrations of 67 and 36 at 25 °C and 0 °C, respectively, and a softening point and brittleness temperature according to Fraass breaking point of 51 and −20 °C, respectively. 0.3% by weight of cellulose fibers was used as a stabilizing additive to prevent segregation. Commercially available up to 10 mm long Viatop-66 ® cylindrical pellets made of cellulose fibers (65%–75% by weight) and bitumen 50/70 was used as a stabilizing additive. The nominal maximum aggregate size was set to 15 mm, the aggregate size distribution together with the limits according to Russian state standard GOST 31015-2002 [38] is presented in Fig. 1. The material is referred in what follows as SMA-15.

Mixing mineral materials, bitumen and fibers of the stone mastic mixture was performed using a Bitumen mixer (Pavement Technology Inc.) at a temperature of 150–155 °C. The optimal mixture was designed using the Marshall method [37]. SMA-15 was modified using capsules with healing agents in an amount of 3% of the bitumen weight. The average capsule size was 1.3 mm, the content of healing agent was 82%–84% by volume. The compressive strength of the capsules was measured in uniaxial compressive tests, as detailed in Ref. [37], with maximum compressive loads being (18 ± 0.5) N.

The capsules were synthesized using the alginate technology described in Ref. [11]. Thiol-containing urethane ARP and SfO were used as healing agents. Dynamic viscosity of ARP and SfO 9.7 and 0.05 Pa·s.

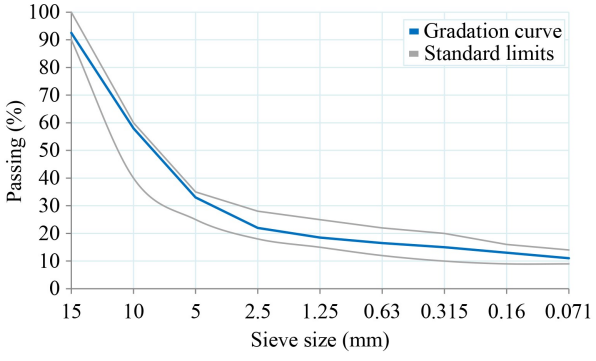

Fig. 1 Gradation curve of SMA-15.

SfO dissolves in bitumen, and ARP glues together by hardening when the capsules are destroyed. When using capsules with ARP in the asphalt concrete mixture, an activator was added in an amount of 5.9% of the bitumen mass. It consisted of technical sulfur, manganese oxide (IV) and tetramethylthiuram disulfide, mixed by weight in a ratio of 6.1:3.7:1 [11]. The determination of the main properties of SMA-15 was carried out according to the methods of Russian state standard GOST 12801-98 [39]. The properties of SMA-15 are presented in Table 1.

2.2 Experimental methods

The SMA-15 specimens were tested in repeated compression and 4PB tests in test-rest-test mode. During the rest periods of 1, 3, or 7 d for both types of tests, the samples were stored at room temperature (20 ± 2) °C and at humidity of 60% ± 2% as representative condition in the field. Higher temperature conditions were not considered to exclude the influence of an additional healing effect from bitumen softening [12]. The scheme of both tests for a series of samples of each type of asphalt is shown in Fig. 2. For characterizing healing efficiency test-rest-test protocols are employed which is a well-established approach, applied by a number of research groups to evaluate healing of various asphalt types [14,19,21].

The cylindrical SMA-15 specimens with a height and diameter of 71.4 mm for quasi-static compression test were manufactured, by placing the required mass of the mixture at 150–155 °C into a mold and compacting it in two stages. First vibration compaction at a frequency of (2900 ± 100) min^{-1}, an amplitude of (0.40 ± 0.05) mm and a vertical load on the mixture of (30 ± 5) kPa, has been applied for 3 min followed by hydraulic press compaction under pressure (20.0 ± 0.5) MPa. The compression test is conducted to determine the load required to fracture a specimen under specified conditions. Prior to testing, a minimum of three specimens is conditioned at a temperature of (20 ± 2) °C. Following thermal stabilization, each specimen is positioned at the center of the lower plate of the press. The press motor is then activated, and loading is applied at a constant plate movement rate of (3.0 ± 0.3) mm/min. The maximum force recorded by the force meter is taken as the breaking load which is subsequently used to calculate the compressive strength. The variation in the compressive strength measurements did not exceed ±0.15 MPa.

The SMA-15 beam specimens were tested for fatigue life using the 4PB test in accordance with AASHTO T 321-14. The sample preparation and testing scheme is shown in Fig. 3.

Hot asphalt concrete mixture at 150–155 °C is placed into the heated form, evenly distributed in the form and

Table 1 Main properties of SMA-15

Parameter	Standard limit (GOST 31015-2002)	SMA	SMA with capsule	
			SfO	ARP
Air void content (%)	1.5–4.5	3.0	1.7	1.8
Water saturation (%)	1.0–4.0	1.9	1.2	1.3
Compressive strength at 20 °C (MPa)/at 50 °C (MPa)	at least 2.2	3.0	2.8	3.6
	at least 0.65	1.1	0.7	1.2
Shear resistance: internal friction coefficient/ shear grip at 50 °C (MPa)	at least 0.93	0.94	0.92	0.93
	at least 0.18	0.56	0.40	0.44
Breaking tensile strength at 0 °C (MPa)	2.5–6.0	2.6	2.2	3.1
Water resistance	at least 0.85	0.92	0.89	0.90

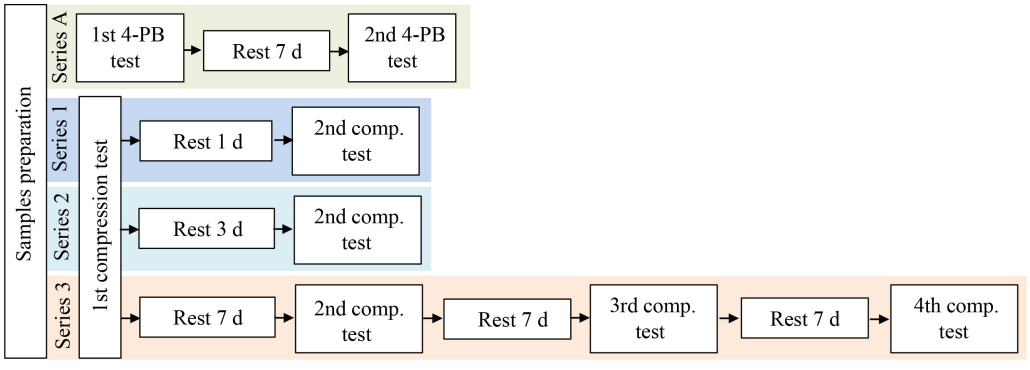

Fig. 2 Scheme compression and bending testing.

compacted using a sector compactor. After cooling to (22 ± 3) °C, the beam specimens were cut from the sample plate, using a sawing machine, so that the edges are parallel, and the final dimensions of the sample are (380 ± 6) mm in length, (50 ± 6) mm in height, (63 ± 6) mm in width. Each specimen is conditioned in a climatic chamber for at least 2 h at a temperature of (10.0 ± 0.5) °C. The test specimen is then installed so that the distance between the centers of the loading clamps is (119 ± 1) mm.

The beam was subjected to repeated sinusoidal bending load in deflection-controlled mode for 250000 cycles with a frequency of 5 Hz with free rotation and horizontal translation at all load and reaction points, providing a central deflection of 0.27 mm in alternating directions, at a temperature of 10 °C. The first 50 bends are used to determine the initial stiffness S_{0i}. The cyclic test data were processed using the indicators presented in Table 2.

The intensity of self-healing was assessed based on the change in the SMA-15 strength as a result of repeated test and rest periods under a given loading scheme. Three repetitions per each test and material were performed. The coefficient of variation for the obtained data did not exceed 1.3%–4.7%.

2.3 Numerical methods

Self-healing asphalt mixtures may be considered as four-phase materials, consisting of air voids, aggregates, binder, and capsules with a healing agent. In this study a micromechanical finite element method (FEM) model is developed in order to evaluate stresses and strains induced in healing capsules during 4PB test. The model is implemented in commercial FE software ABAQUS [40]. The particular focus is on the effect of damage accumulation in asphalt on stresses and strains induced in capsules with healing agent. The micromechanical model is developed for the SMA-15 mixture containing capsules with ARP healing agent, following a methodology proposed by Refs. [37,41].

The model geometry, along with loading and boundary conditions used is shown in Fig. 4(a). In the model, the asphalt material is composed of four phases: an elastic aggregate phase, an elastic capsules phase, an air voids phase and an elastic matrix representing asphalt mortar. The phases of the aggregates, capsules and air voids are represented by randomly distributed elastic spherical particles in the elastic matrix, representing the mortar. The aggregate size distribution follows the gradation for SMA-15 presented in Fig. 1. Aggregates with sizes smaller than 5 mm were attributed to the mortar phase and not modeled explicitly. Air voids are modeled as spheres of 2 mm diameter, occupying 3.2% of the mixture volume.

The numerical study is focused on the case of SMA-15 with a capsules content of 0.49% by volume of the mixture, which corresponds to the capsules content of 3.0% by weight of the binder. Figure 4(b) shows the particles randomly distributed within the representative volume element (RVE) space, while Table 3 shows the composition of the different phases in RVE.

The mortar is assumed to be represented by isotropic linear elastic material, with its properties described by Young's modulus, E, and Poisson's ratio, ν. In contrast to previous studies, e.g., Refs. [37,41], where the mortar phase was modeled as linear viscoelastic material, the

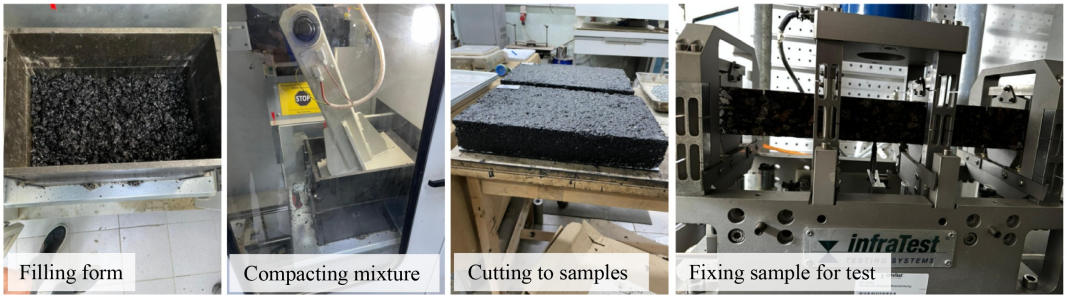

Fig. 3 Scheme preparing sample and 4PB testing

Table 2 Parameters for 4PB test

Equation No.	Parameter	Formula	Note
(1)	Maximum tensile stress (MPa)	$\sigma = \frac{LP}{bh^2}$	L is beam length between external clamps, 0.357 m; P is test load, N; b is average sample width, m; h is average height of the sample, m
(2)	Maximum tensile strain (m/m)	$\varepsilon = \frac{12\delta h}{3L^2 - 4a^2}$	δ is maximum deflection in the center of the beam, m; a = 0.119 m is the distance between the inner clamps
(3)	Bending stiffness (Pa)	$S = \frac{\sigma}{\varepsilon}$	σ is maximum tensile pressure, MPa ε is maximum tensile strain, m/m
(4)	Number of cycles to failure	$N_f = \frac{250\text{E}3 \cdot \ln 2}{\ln \frac{S_0}{S_{n=250\text{E}3}}}$	S_0 and $S_{n=250\text{E}3}$ is initial beam stiffness and beam stiffness at cycle 250E3, respectively. The equation assumes that the evolution of S with load cycles is defined by $S(n) = S_{0i} \cdot e^{-\beta \cdot n}$.

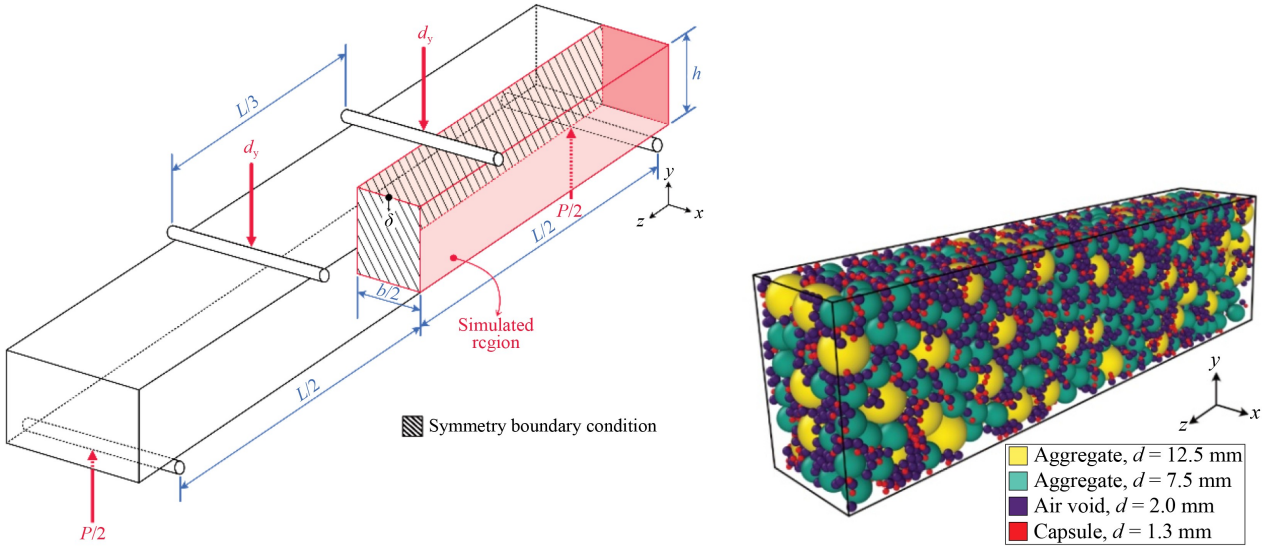

(a) (b)

Fig. 4 (a) 4PB schematic showing the model and symmetry boundary conditions and (b) the random distribution of spherical particles in the modeled region.

Table 3 The volumetric composition of asphalt mixture in the FE model

Element	Sphere diameter (mm)	Volume proportion (%)
Matrix	–	45.0
Aggregates	12.5	29.5
	7.5	21.8
Capsules	1.3	0.5
Air void	2	3.2

temperature and load rate effects on creep and relaxation properties of asphalt are not of interest presently. The attention is rather focused on the asphalt performance under cyclic loading in a 4PB test. Accordingly, linear elastic representation for mortar is chosen for computational efficiency.

To capture the effect of damage accumulation on the stresses and strains induced in the capsules, a simple strain-softening model is employed assuming that the damage accumulation in mortar is governed by the magnitude of the maximum tensile strain induced. As outlined in Subsection 2.2, 4PB tests were conducted for 250000 cycles. However, explicitly modeling damage progression over such a large number of cycles is computationally prohibitive. As an alternative approach, the first cycle of the 4PB test is modeled and it is assumed, that the damage accumulation in the mortar is governed by the magnitude of tensile strain induced. Accordingly, the elements in the mortar subjected to the first principal strain, ε_1, above a certain threshold, ε_f, are expected to fail at cycle $N = 250000$. The failure of the given element is modeled by reducing its Young's modulus to 1% of the original mortar modulus.

The strain-softening model outlined in the previous paragraph is implemented as a post-processing subroutine in ABAQUS. The first loading cycle in the 4PB test is conducted, assuming no damage is accumulated during the cycle. For the 250000 cycle, however, the USDFLD subroutine in ABAQUS is activated, identifying mortar phase elements with $\varepsilon_1 \geqslant \varepsilon_f$ and assigning them a stiffness value equal to 1% of the undamaged mortar modulus. This 99% reduction of the mortar stiffness is assumed to represent failure of the given mortar element. Once the damage is distributed throughout the mixture, the FE modeling of the 4PB test on the damaged asphalt is carried out with the USDFLD subroutine deactivated to study the effect of damage on capsules containing the healing agent. To identify the capsules sharing nodes with the damaged mortar elements, a Python script was developed to identify the damaged capsules by using the radius and coordinates of the capsules, and comparing them to the nodal coordinates of the damaged mortar phase. The script employs a nearest neighbor searching algorithm developed in Ref. [42] as implemented in the Python package SciPy [43].

The flowchart of the modeling process is illustrated in Fig. 5, where E and ν are the stiffness and Poisson's ratio respectively while the subscripts m, a, c refer to the matrix, aggregates and capsules, respectively.

The aggregate, air voids and healing capsules phases are generated in the molecular dynamics software LAMMPS [44], following the methodology presented in Ref. [18]. In this method the particles representing the aggregates, air voids and capsules are dropped under action of gravity into a rectangular prism with the dimensions of $2L$, $1.1h$, and $1.1\frac{b}{2}$. The locations and radii of the spheres are then imported into ABAQUS

where the nodes are merged with the nodes of the mortar phase. Finally, the model is cut to the dimensions shown in Fig. 4(a), i.e., L, h, and $\frac{b}{2}$. The elastic properties of the aggregates were assumed the same as for limestone [45], with Young's modulus, E = 39.3 GPa and Poisson's ratio ν = 0.23. The Young's modulus for the capsules was set to E_c = 3 GPa and their Poisson's ratio to ν_c = 0.495, following the findings by Ref. [37]. The elastic properties of the mortar phase were identified as to result in the same effective asphalt beam stiffness as the one measured during the first load cycle in 4PB test, i.e., $S_{N=1} = 4940$ MPa. The damage threshold, ε_f, was identified as to give the same reduction of effective asphalt beam stiffness after 250000 cycles as measured experimentally for SMA-15 with ARP modifier, i.e., $S_{N=250E3} = 0.64 S_{N=1}$.

The models were meshed with tetrahedral quadratic elements, with the elements sizes ranging between 0.002 and 4.1 mm resulting in 1301881 elements. The resulting FE mesh is shown in Fig. 6. Reducing the maximum size of elements to 3.1 mm (1602526 elements) and 2.6 (1969122 elements) results in less than 1.5% change in calculated stiffness of the model.

3 Results and discussion

3.1 Experimental results

To assess self-restoration efficiency a relative comparison of the asphalt strength before and after rest periods is used [37,43–48]. This indicator allows evaluating the degree of self-healing of asphalts incorporating different modifiers or under increased temperatures [12,49,50]. The specimens are subjected to mechanical tests where damage is introduced to the material and the induced damage characteristics will vary with the test method and the load level chosen. In some studies, for example, when splitting tests are used [29,30,49,51], loading of specimens is carried out until macro-cracks form, resulting sometimes in specimens being broken into two parts. Different fracture mechanisms, types and scales of defects create different initial conditions for the self-healing processes to occur. It is obvious that the effectiveness of the self-healing modifier will differ under different initial conditions.

In this study, a comparison of self-healing processes is performed for two distinct types of loading: monotonically increasing load in compressive and cyclic loading in

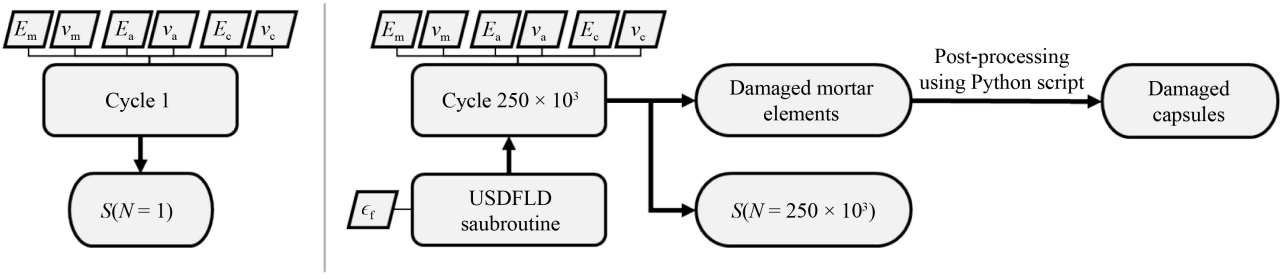

Fig. 5 Flowchart describing the modeling process to calculate the stiffness of the mixture when damage is included as well as to identify the damaged mortar elements and capsules.

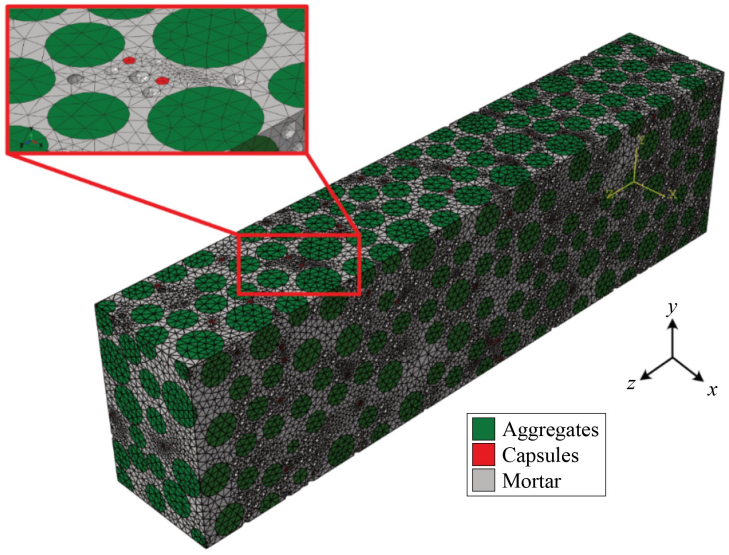

Fig. 6 The mesh for the model used in the 4PB simulation.

4PB bending tests. Both tests are conducted repeatedly with rest periods between the tests, as explained in detail in Subsection 2.2. The evolution of specimen strength during repeated static compression tests is presented in Fig. 7.

As seen in Fig. 7 the three SMA types have significantly different strength during the first test in the series. It has been previously shown [37,52,53] that capsules in the material are destroyed due to formation of defects and release the healing agent. The healing effect in asphalt concrete can be achieved both by the spontaneous "entanglement" of molecules of organic compounds in the zone of bond rupture that occurred during the formation of a crack, and by the gluing of crack surfaces with the formation of new adhesive bonds due to the modifier. In case of SfO, the modifier softens the binder and promotes the spontaneous entanglement of its molecules. ARP on the other hand, allows the formation of new adhesive bonds in a two-stage process, where in the first stage the ARP (adhesive) moves into the material (substrate) following the orientation of molecules in the boundary layer. In the second stage the adhesive and substrate interact with the participation of van der Waals forces and/or with the formation of chemical bonds [18].

On the 1st day after the first test, the strength of SMA-15 is 65% of the initial strength, the one of SMA-15 with encapsulated SfO is 63%, and the one of SMA-15 with encapsulated ARP is 72%. After the 3rd day of rest after the first test, a contribution of the self-healing process is observed. After 7 d rest, the strength of SMA-15 and SMA-15 with encapsulated SfO increased to 2.2 MPa (i.e., 75% and 82% of the initial strength, respectively), while the strength of SMA-15 with encapsulated ARP was 3.27 MPa, which corresponds to 91% of the initial strength.

Further repetitions of compression tests show a decrease of strength due to accumulation of defects in the structure of the material. For SMA-15, the fourth compression test showed a strength equal to 53% of the initial value. This indicates low self-healing efficiency of the bitumen binder alone [12,54,55]. The use of encapsulated SfO, on the other hand, increases the self-healing effect in asphalt. After the fourth compression test for SMA-15 with encapsulated SfO the strength is 66% of the initial value whereas for asphalt with encapsulated ARP the ultimate strength is 85% of the initial value. Thus, the use of encapsulated ARP appears to create a greater resistance to the formation of defects in asphalt due to the self-healing effect of ARP.

It is also evident from Fig. 7 that repeated compression tests of samples lead to a decrease in strength from accumulating structural defects, and the intensity of this process can be used to judge the speed at which the critical state is reached. A critical state is defined in this study as the point when the specimen reaches a minimum strength acceptable according to standard. The slope of the strength-time dependence shows that the rate of defect accumulation during repeated compression tests for SMA-15 with an encapsulated modifier is less than for the SMA-15. According to Russian state standard GOST 31015-2022 [38], the minimum acceptable compressive strength for SMA-15 is 2.2 MPa. As seen in Fig. 7, both for SMA-15 and for SMA-15 with SfO, the strength will be below 2.2 MPa already at 3rd test repetition while for SMA-15 using encapsulated ARP, the measured strength is above 3 MPa even at 4th compressive test.

The results of the cyclic 4PB are presented in Fig. 8. As seen in Fig. 8, the bending stiffness of asphalt decreases gradually with loading cycles, indicating that damage is introduced into the material. The rate of this stiffness reduction, illustrated by the curve AB in Fig. 8, is, however, different for different types of asphalts. Namely, the stiffness of traditional asphalt after 250000 load cycles is 60% of its initial stiffness, while the presence of SfO capsules reduces this figure to 52%. For asphalt with encapsulated ARP, due to the presence of the activator, the rate of reduction in stiffness decreases, resulting in 65% of the initial value after testing. The self-healing process during 7 d of rest of the material samples is accompanied by an increase in stiffness, cf. points B

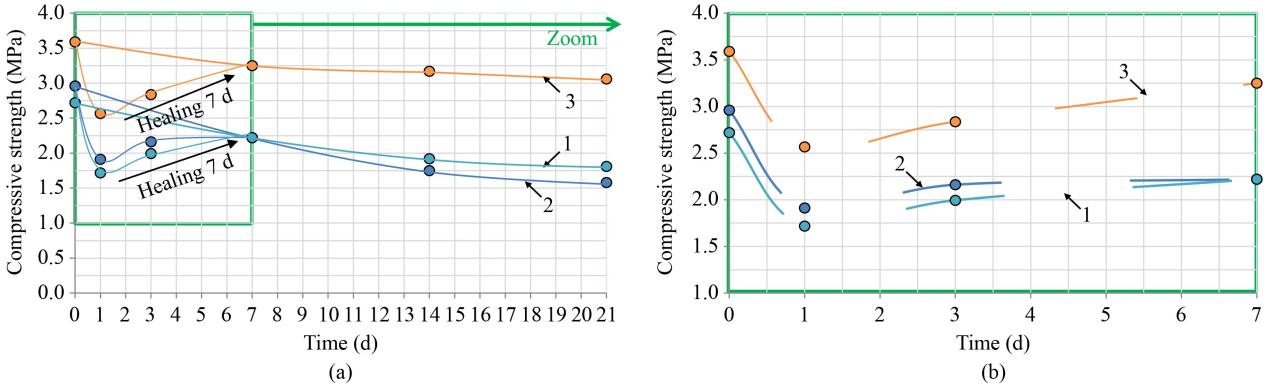

Fig. 7 (1) Compressive strength in repetitive monotonic compression tests at 20 °C of SMA-15, (2) SMA-15 with encapsulated SfO and (3) SMA-15 with encapsulated ARP: (a) full scale; (b) zoomed.

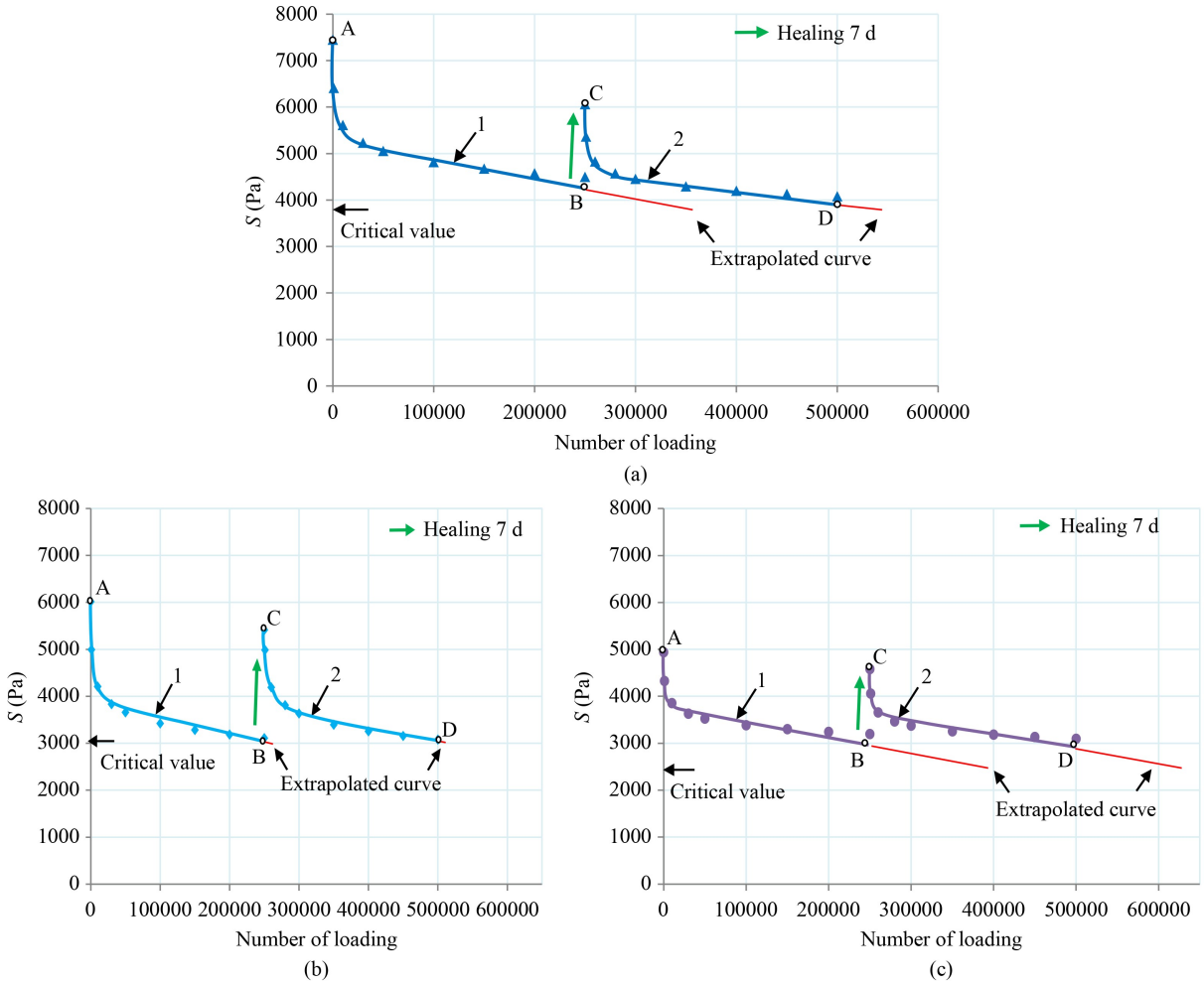

Fig. 8 Bending stiffness during cyclic test at 10 °C for SMA-15: (a) SMA-15 with encapsulated SfO; (b) SMA-15 with encapsulated ARP; (c) before (1) and after (2) rest period.

and C Fig. 8. The stiffness of asphalt without capsules is restored to 81% of the initial value in 7 d due to the bitumen's own self-healing potential [12,54]. The use of encapsulated SfO allows to restore the bending stiffness to 90% of the initial value, and the use of encapsulated ARP to 93%. SfO dissolves in the defect area and increases the rate of spontaneous entanglement of bitumen molecules. ARP, flowing out of the capsules, diffuses into the matrix where the activator was dissolved, the interaction reaction occurs and it hardens, gluing the defect area. This proves that the contribution of ARP and SfO to the self-healing process is significant. It is also important that the repaired structure of asphalt after self-healing is able to resist further loads. This is evaluated by applying additional 250000 load cycles in the 4PB test. After the second series of 250000 cycles, the bending stiffness of SMA-15 is 55% of the initial value, whereas the stiffness of SMA-15 with encapsulated SfO is 51%, and the stiffness of SMA-15 with encapsulated ARP is 63%. Conventionally, a decrease of asphalt stiffness to 50% of the initial value is taken as a critical point corresponding to failure. Using Eq. (4) to extrapolate the curves shown in Fig. 8, results in the predicted fatigue life of 343000 cycles for SMA-15, and introducing a 7 d healing period after 250000 cycles increases the fatigue life to 538 000 cycles. For SMA-15 with encapsulated SfO the fatigue life is estimated to be 263000 cycles, and 7 d healing period increases it to 509000 cycles. The effect of the healing period on the fatigue life of SfO modified material is thus even smaller than for the standard SMA-15. This may be explained by an excess of light fractions that have penetrated the matrix from the capsules, excessively softening the bitumen. For SMA-15 with encapsulated ARP fatigue life is estimated to be 398000 cycles and 621000 cycles without and with healing period correspondingly.

The efficiency of self-healing will depend on the characteristics of damage induced in asphalt. After testing material samples under quasi-static compression and cyclic bending loads, the specimens contain populations of defects which differ according to their spatial distribution, sizes and volume. This affects the efficiency of self-healing. The self-healing efficiency in Fig. 9 is quantified through the healing index calculated by the

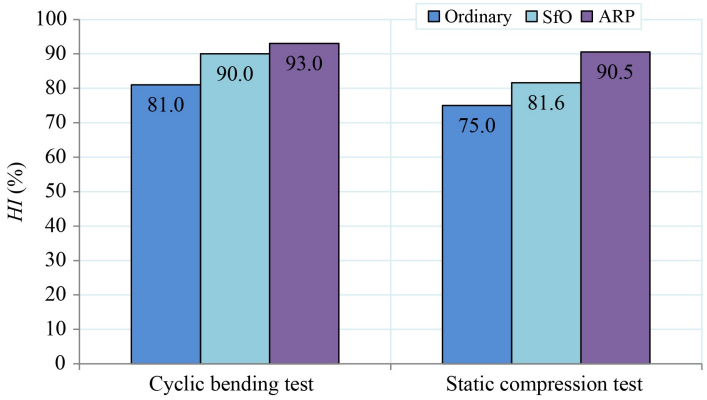

Fig. 9 Self-healing effect after quasi-static compression and cyclic bending test for SMA-15, SMA-15 with encapsulated SfO and encapsulated ARP.

following expression:

$$HI = \frac{I_h}{I_0} \cdot 100\%, \quad (1)$$

where I_0 measured strength or stiffness of SMA-15 and I_h strength or stiffness of SMA-15 measured after rest period.

As seen in Fig. 9, a greater self-healing effect is observed when using encapsulated ARP in asphalt under both quasi-static compression and cyclic bending loads. It is also observed, that the difference in healing efficiency of the unmodified SMA-15, SMA-15 containing SfO and ARP agents is significantly smaller in case of cyclic tests. This may be attributed to smaller crack sizes introduced during the cyclic tests, which is also in line with the self-healing effect being generally higher for the damage under cyclic bending loads than after monotonic compression strength tests. The stresses and strains induced in cyclic 4PB tests are significantly below the ones induced in monotonic compression strength tests, resulting in smaller cracks. Therefore, the crack edges are closer to each other, and self-healing is more effective. Accordingly, a more significant portion of the introduced defects will be healable. The obtained results correspond with the results of other authors [54–57].

3.2 Numerical results

In this section, results from the FE model for SMA-15 with ARP subjected to 4PB test are presented. It was found that setting Young's modulus of mortar to 0.790 GPa results in an asphalt beam bending stiffness of 4.944 GPa, which agrees with the experimental findings presented in Fig. 8(c). Similarly, setting the threshold to $\varepsilon_f = 2.2 \times 10^{-3}$ and distributing damage according to the method outlined in Subsection 2.3, makes the asphalt beam bending stiffness drop to 3.179 GPa which fits the observations in Fig. 8(c) for N = 250000. In Fig. 10, the measured evolution of the bending stiffness for the asphalt beam is compared to the numerical predictions obtained at N = 1 and N = 250000. As seen, the experimental and numerical results are in close agreement. Furthermore, in order to evaluate the effect of mesh size on the simulation results, the numerical results in Fig. 10 are presented as obtained with 3 different mesh densities. The influence of the element size on the back-calculated stiffness was found to be small with beam stiffness varying less than 1.5% at N = 250000.

In the following, the attention is focused first on the stress-state induced in the asphalt beam during the 4PB test. In Fig. 11 the distributions of first principal stresses and strains are shown as obtained by the model for the first load cycle of the 4PB test.

Color legends for the maximum principal strains are adjusted for visibility, by omitting the elements subjected to strains below 5×10^{-5} and above 3.06×10^{-2}. As may be seen, the material inhomogeneity affects both stress and strain distributions profoundly. While tensile stresses are somewhat higher at the bottom of the specimen, as would be expected for a homogeneous elastic beam, there are also some local tension zones distributed through the material, arising due to mechanical interaction between different phases. As also seen in Fig. 11(b), the first principal strains are dominantly localized in the mortar phase, as may be expected based on the differences in the Young's module of mortar and aggregates. In Fig. 12 the

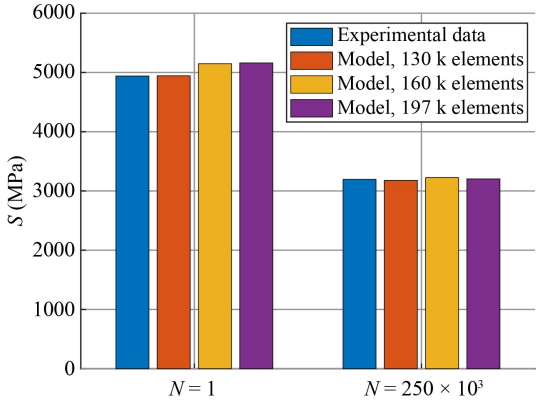

Fig. 10 The stiffness calculated at N = 1 and N = 250000 for the models with different mesh sizes.

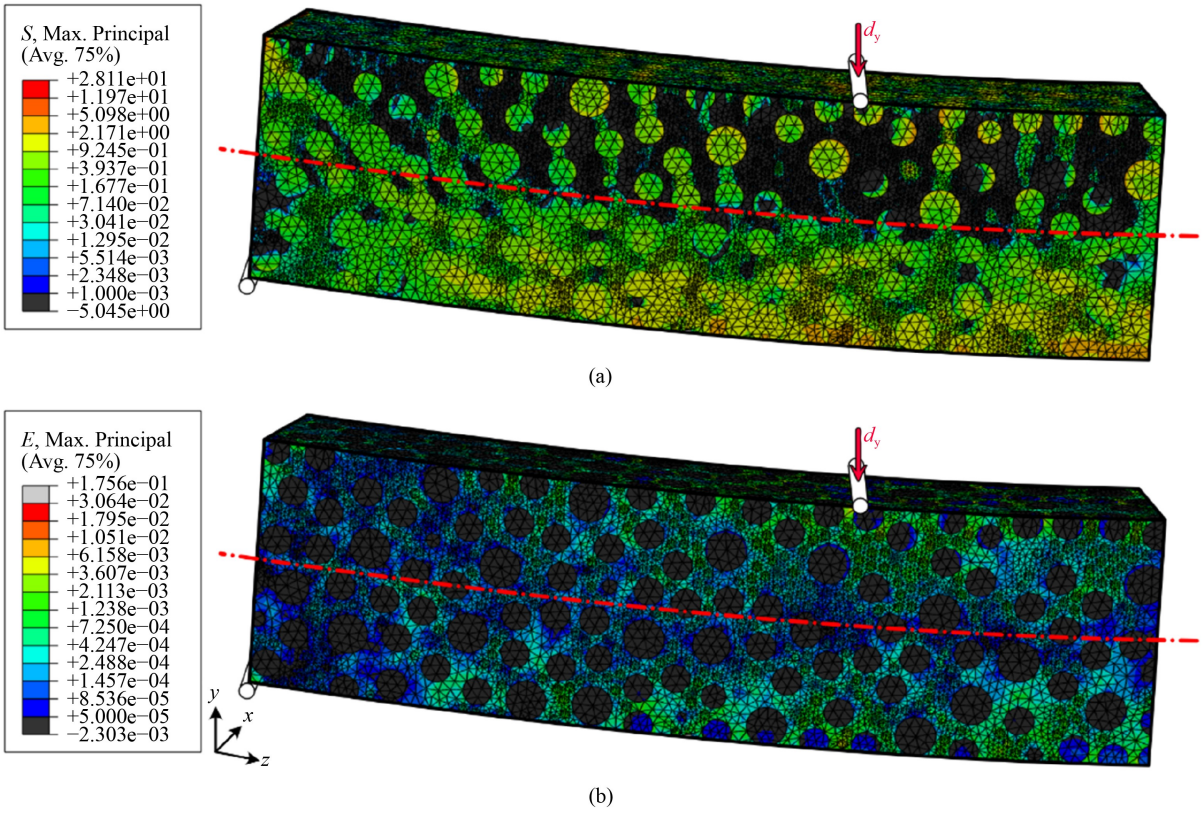

Fig. 11 Maximum principle: (a) stresses and (b) strains distributions in a quarter of the asphalt beam at $N = 1$.

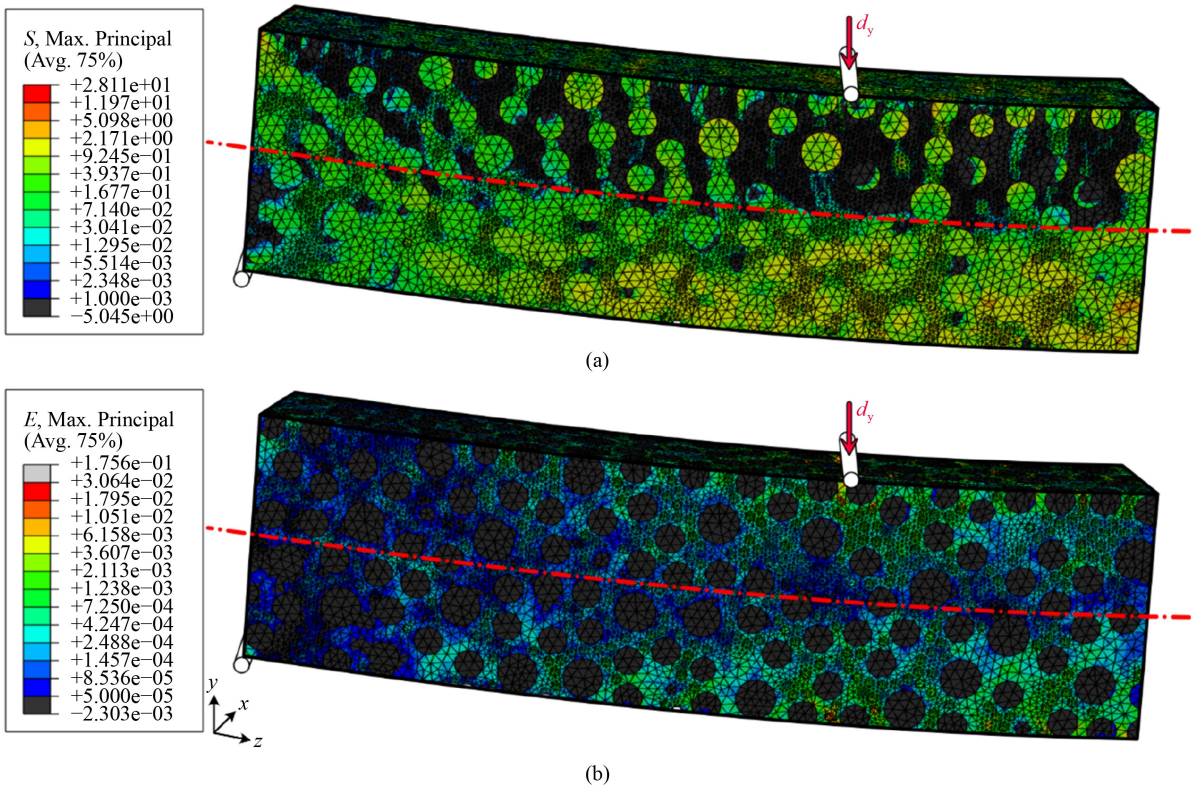

Fig. 12 Maximum principle: (a) stresses and (b) strains distributions in the asphalt beam at $N = 250000$.

distribution of first principal stresses and strains are shown as obtained by the model at load cycle N = 250000, i.e., after the damage has been introduced to the material.

As may be seen, the distributions are qualitatively similar to the ones observed in Fig. 11. At the same time, due to accumulation of damage, somewhat higher concentrations of tensile stresses and strains appear in Fig. 12, in particular at the bottom of the specimen. This is expected, as part of the mortar phase is now weakened and does not fully support the load anymore. The distribution of damage is shown in Fig. 13.

Figures 13(a) and 13(b) demonstrate that the damage is primarily located at the bottom of the asphalt beam and close to the point of maximum deflection. At the same time there is also a considerable amount of damage close to the upper surface of the beam, due to local tensions arising in mortar as illustrated in Fig. 11(b). The mortar phase close to the beam's neutral axis accumulates virtually no damage. The resulting volume of damaged mortar is 2 358 mm^3 which corresponds to 2.1% of the total mortar volume. Also, in Fig. 13(c) a close-up view of the damaged mortar zone is shown along with healing capsules embedded in it. These capsules were identified with the procedure outlined in Subsection 2.3. The total volume of capsules embedded in the damaged mortar is 94 mm^3 which corresponds to 8.4% of the total volume of capsules.

For the capsules to be efficient in restoring the damage induced in asphalt mixtures, their strength should be optimized in a way that they do not fail under the normal service conditions and release the healing agent only when the material is damaged in their vicinity. In Ref. [37] micromechanical modeling was employed to evaluate the stresses and strains induced in healing capsules during compaction at normal service conditions as well as when cracks had formed in the vicinity of the capsules. It was observed in that study, that crack formation results in approximately 40% increase in tensile stresses induced in the capsules close to the crack tip. Accordingly, the micromechanical modeling allowed to identify the desired strength of the capsules, ensuring that they survive compaction and normal service conditions and release the healing agent only when the crack is formed near a capsule. However, the effect that a distributed fatigue damage has on the healing capsules has not been evaluated yet.

As the stresses and strains induced in the capsules vary in a wide range depending on their location in the mixture, the capsules propensity to breakage is best evaluated from a statistical point of view. In Fig. 14, cumulative probability distributions of the first principal stresses and strains induced in healing capsules during beam bending is presented.

For a given stress level, σ_c, the cumulative probability, $F_\sigma(\sigma_c)$ is calculated according to the following equation:

$$F_\sigma(\sigma_c) = \frac{n_{\sigma \leqslant \sigma_c}}{N_{\text{total}}} \cdot 100\%. \quad (2)$$

where $n_{\sigma \leqslant \sigma_c}$ is the number of capsules subjected to stresses less than or equal to σ_c, and N_{total} is the total number of capsules in the volume. As seen from Eq. (6), $F_\sigma(\sigma_c)$ denotes the share of the capsules subjected to stresses below σ_c. For example, if for a given loading scenario $F_{\sigma_1}(10\text{ MPa}) = 90\%$, where σ_1 is the maximum principal stress, 10% of the capsules are subjected to tensile stresses above 10 MPa. In the analysis presented in Fig. 14, the healing capsules are divided into two groups: those embedded in the mortar regions, where $\varepsilon_1 \geqslant \varepsilon_f$, and those embedded outside those regions.

The results are presented as percent of the capsules' total volume. In Fig. 14, the cumulative distribution of the maximum tensile stresses and strains within the capsule phase are shown as obtained at $N = 1$ and $N = 250000$.

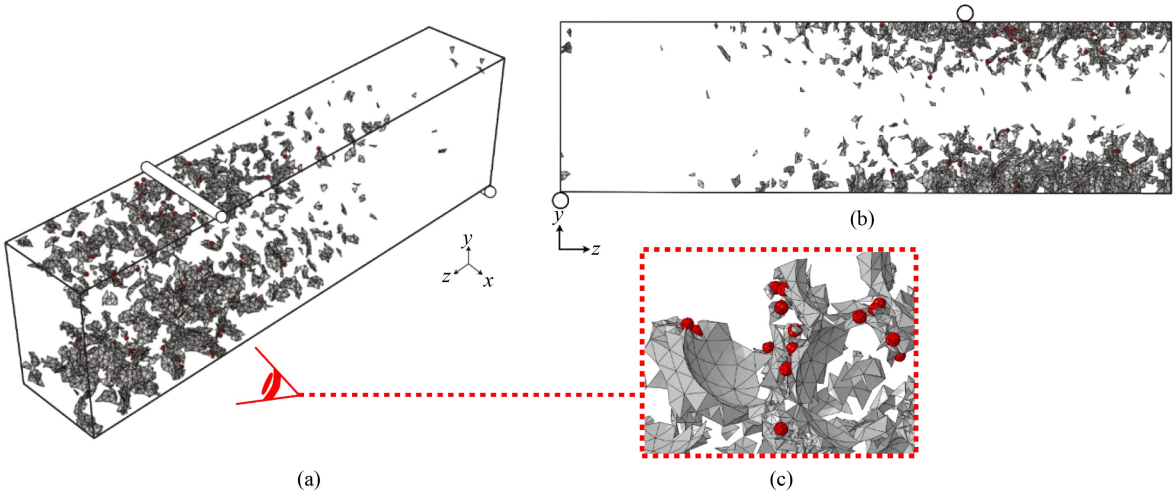

Fig. 13 Distribution of damage in the mortar phase after N = 250000: (a) 3D view; (b) side view; (c) close up view showing damage zone with capsules embedded in damaged mortar.

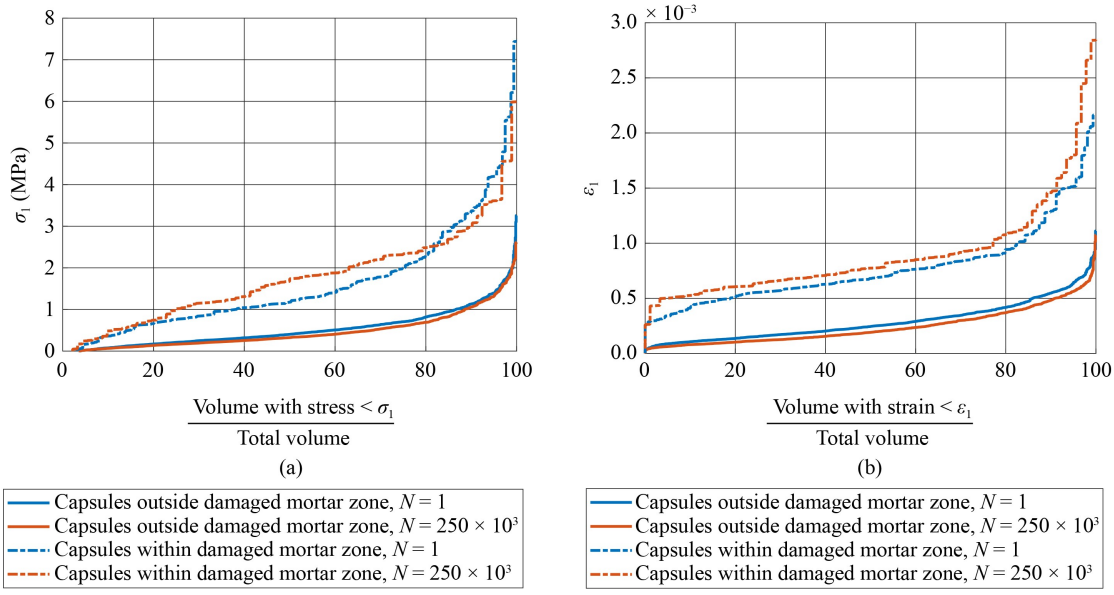

Fig. 14 Cumulative probability distributions of (a) stress; (b) strain in the capsules outside and within the damaged mortar zone.

Considering the results at $N = 1$, capsules located close to the mortar regions subjected to $\varepsilon_1 \geqslant \varepsilon_f$ experience generally higher tensile stresses and strains as compared to the capsules outside of those regions. In particular, 50% of the capsules located in the mortar with $\varepsilon_1 \geqslant \varepsilon_f$ are subjected to $\sigma_1 \geqslant 1.2$ MPa and $\varepsilon_1 \geqslant 7 \times 10^{-4}$, whereas the corresponding values for the capsules located outside of those mortar regions are 0.4 MPa and 2.5 $\times 10^{-4}$. This considerable difference in the tensile loads experienced by the capsules in different regions of asphalt mixture potentially allows to optimize the material design of the capsules to ensure their timely activation. For example, according to Fig. 14(a) optimizing the capsules such that they survive the repeated tensile stresses of 1.2 MPa ensures that outside the mortar regions where the damage is forming only small proportion (approximately 10%) of the capsules will break. Within the region susceptible to damage at least 50% of capsules will break, and even higher proportion of capsules may break due to stress concentrations when micro-cracks form in the vicinity of the capsules.

It is also of interest to evaluate the effect of damage on the stresses and strains induced in the capsules. This is examined in Fig. 14, where the cumulative distributions of the maximum tensile stresses and strains are shown for $N = 250000$. It has to be pointed out that damage in the capsules has not been modeled explicitly in this study, in order to allow a representative comparison with the non-damaged mortar case. As seen in Fig. 14, after damage accumulation, the tensile stresses and strains experienced by the capsules in the damaged zone increase, since 50% of the capsules are now subjected to $\sigma_1 \geqslant 1.9$ MPa and $\varepsilon_1 \geqslant 8 \times 10^{-4}$. Thus, the location of the capsules in the damage region increases their breaking probability significantly. At the same time, for the capsules located outside the damaged zone, the opposite is true with both tensile stresses and strains reduced according to the stress redistribution within the specimen. This results in $\sigma_1 \geqslant 0.25$ MPa and $\varepsilon_1 \geqslant 2 \times 10^{-4}$ for 50% of the capsules. Accordingly, this reduces the probability of breaking the capsules outside the damaged region and, therefore, the probability of their premature activation.

4 Conclusions

In this study SMA-15 modified with capsules containing healing agents were evaluated experimentally and numerically. In particular the efficiency of two healing agents, thiol-containing urethane ARP and SfO, was evaluated.

Self-healing of SMAs was studied under monotonically increasing compression at (20.0 ± 2) °C and cyclic 4PB at (10.0 ± 0.5) °C. Both loading conditions and healing agents strongly influenced healing efficiency. Load mode effects were linked to the type of damage formed: compressive tests produced larger defects, which healed less effectively, while cyclic bending introduced smaller defects in the material which led to better damage recovery. Consequently, SMAs showed greater self-healing after cyclic bending tests than after monotonic compression. Among healing agents, ARP outperformed SfO due to its adhesive action, while the latter only softened bitumen. Encapsulated ARP restored up to 93% of strength and stiffness, SfO up to 90%, and unmodified SMA 81%. After healing, asphalt with encapsulated ARP withstood 15% and 22% higher loads than SMA without and with encapsulated SfO, respectively.

Micromechanical finite element modeling was used to study the stress state in SMA-15 with ARP capsules

during 4PB. A simple strain softening model was incorporated into the FE model to account for damage formation during cyclic loading. The numerical results show that, the heterogeneity produces local zones of tensile stresses and strains distributed more or less through the whole specimen volume. Those zones are concentrated in the central zone between the loading points of the beam and the tension is somewhat higher at the specimen bottom. After 250000 cycles, about 2% of the mortar volume was damaged in the FE model, with 8.4% of capsules intersecting these regions. As shown by the authors in an earlier study [37], the formation of cracks in the vicinity of capsules results in a significant increase of tensile stresses due to stress concentrations at the crack tips close to the capsules. Accordingly, a significant proportion of the capsules embedded in the damaged mortar regions may be expected to break.

To evaluate whether there is a risk of premature capsule breakage, activation stresses and strains in capsules were examined before and after specimen damage initiation. It was observed that even prior to the initiation of damage, the capsules in the mortar zone, where damage will initiate, were subjected to stresses significantly higher than those outside the damage regions. In particular, the stress level corresponding to 50% cumulative probability was 3 times higher for the capsules in the damaged regions. After damage initiation, the tensile stresses in the capsules located in the damaged mortar regions increased further by approximately 60% while the stresses and strains in the capsules outside the damaged regions were reduced. The obtained numerical results indicate that there is a considerable difference in stresses and strains for the capsules located inside and outside the damage regions. Accordingly, it is feasible to tailor the strength of the capsules such that they survive service loads yet fracture upon local damage.

It has to be pointed out that in order to fully quantify the effect of healing capsules in asphalt, the developed FE model needs to be updated to incorporate the healing of damage near the broken capsules. This development was, however, outside the framework of this study and will be done as a part of future work. The limiting sizes of cracks that can be healed by encapsulated modifiers as well as the effect of environmental loads on materials healing potential should also be investigated.

Acknowledgements Part of this work was financially supported by the Russian Science Foundation (No. #22-79-10051). Tests were carried out using research equipment of The Head Regional Shared Research Facilities of the Moscow State University of Civil Engineering.

Competing interests The authors declare that they have no competing interests.

References

1. Emtiaz M, Imtiyaz M N, Majumder M, Idris I I, Mazumder R, Rahaman M M. A comprehensive literature review on polymer-modified asphalt binder. CivilEng, 2023, 4(3): 901–932
2. Milad A, Ali A S B, Yusoff N I. A review of the utilisation of recycled waste material as an alternative modifier in asphalt mixtures civil. Engineering Journal, 2020, 6: 42–60
3. Atrash K E, Assaf G. Evaluating factors influencing asphalt road construction quality in high temperature condition. Journal of Civil Engineering, Science and Technology, 2019, 10(1): 75–81
4. Chen C, Deng Y, Li M, Shi X. Investigation of key climatic factors affecting asphalt pavement roughness in different climate regions. Transportation Research Part D, Transport and Environment, 2023, 122(C): 103877
5. Sebaaly H, Riviera P P, Varma S, Maina J W, Santagata E. Performance-based assessment of rutting resistance of asphalt mixes designed for hot climate regions. International Journal of Pavement Engineering, 2022, 3(7): 2448–2459
6. Khan K, Ahmad W, Amin M N, Khan S A, Deifalla A F, Yousef M. Research evolution on self-healing asphalt: A scientometric review for knowledge mapping. Reviews on Advanced Materials Science, 2023, 62(1): 20220331
7. Abejón R. Self-healing asphalt: A systematic bibliometric analysis for identification of hot research topics during the 2003–2018 period. Materials, 2021, 14(3): 565
8. Zghoundi Y, Boutgoulla M, Akkouri N, Taha Y, Hakkou R, El-Azdi K, Kebir M, Ben Salem Y A, Edfouf Z. Self-healing microencapsulation technology for asphalt pavements: A review. NanoWorld Journal, 2023, 9(S2): S341–S349
9. Pompigna, A, Mauro R. Smart roads: A state of the art of highways innovations in the smart age. Engineering Science and Technology, an International Journal, 2022, 25: 100986
10. Almutairi H, Baaj H. Evaluating self-healing behaviour of asphalt binders modified with phase-change materials, polymers and recycled glass powder. Polymers, 2023, 15(8): 1934
11. Inozemtcev S, Korolev E. Active polymeric reducing agent for self-healing asphalt concrete. Materials Science and Engineering, 2021, 1030(1): 012002
12. Inozemtcev S S, Korolev E V, Do T T. Intrinsic self-healing potential of asphalt concrete. Magazine of Civil Engineering, 2023, 123(7), 12308
13. Ani O J, Shafabakhsh G, Mirabdolazimi S M. Investigation of rheological characteristics of powdered activated carbon modified bitumen for use in self-healing mechanism of asphalt concrete. Journal of Rehabilitation in Civil Engineering, 2024, 12(2): 58–68

14. Al-Mansoori T, Norambuena-Contreras J, Micaelo R, García A. Self-healing of asphalt mastic by the action of polymeric capsules containing rejuvenators. Construction and Building Materials, 2018, 161: 330–339
15. Micaelo R, Freire A C, Pereira G. Asphalt self-healing with encapsulated rejuvenators: effect of calcium-alginate capsules on stiffness, fatigue and rutting properties. Materials and Structures, 2020, 53(1): 20
16. Cabette M, Micaelo R, Pais J. Self-healing asphalt roads: evaluation of calcium alginate capsules with bio-oil. Transportation Research Procedia, 2023, 72: 688–695
17. Norambuena-Contreras J, García A. Self-healing of asphalt mixture by microwave and induction heating. Materials & Design, 2016, 106: 404–414
18. Inozemtcev S, Korolev E, Do T T. Choice of healing agent for self-healing asphalt concrete. Materials, 2023, 16(24): 7542
19. Chen S, Liu Q, Bi Y, Yu B, Zhang J. Self-healing effect of various capsule-core materials on asphalt materials. Advances in Civil Engineering, 2022, 2022(3): 1–17
20. Wang H, Yuan M, Wu J, Wan P, Liu L. Self-healing properties of asphalt concrete with calcium alginate capsules containing different healing agents. Materials, 2022, 15(16): 5555
21. Alvaro García A, Schlangen E, Ven M. Properties of capsules containing rejuvenators for their use in asphalt concrete. Fuel, 2011, 90(2): 583–591
22. Li L, Guo Z, Ran L, Zhang J. Study on low-temperature cracking performance of asphalt under heat and light together conditions. Materials, 2020, 13(7): 1541
23. Nguyen M L, Chupin O, Blanc J, Piau J M, Hornych P, Lefeuvre Y. Investigation of crack propagation in asphalt pavement based on APT Result and LEFM analysis. Journal of Testing and Evaluation, 2020, 48(1): 161–177
24. Wang M, Li S C, Liu R T, Zhang C Y, Zhu Z J, Zhang L Z, Bai J W. Research on pavement cracking possibility based on the load mechanical response. Science China. Technological Sciences, 2023, 66(12): 3549–3561
25. Elseifi M A, Baek J, Dhakal N. Review of modelling crack initiation and propagation in flexible pavements using the finite element method. International Journal of Pavement Engineering, 2018, 19(3): 251–263
26. Huang W, Li B, Huang M. Evaluation of self-healing of asphalt mixture through four-point bending fatigue test. Journal of Building Materials, 2015, 18(4): 572–577 (in Chinese)
27. Inozemtcev S, Korolev E. Indicators of the effectiveness of self-healing asphalt concrete. E3S Web of Conferences. EDP Sciences, 2019, 97: 02007
28. Hasaninasab S. Investigating the healing capability of asphalt modified with nano-zycotherm and forta fibers. Case Studies in Construction Materials, 2019, 11: e00235
29. Zhang F, Sun Y, Kong L, Falchetto A C, Yuan D, Wang W. Study on multiple effects of self-healing properties and thermal characteristics of asphalt pavement, 2024, 14(5): 1313
30. Shu B, Bao S, Wu S, Dong L, Li C, Yang X, Norambuena-Contreras J, Liu Q, Wang Q. Synthesis and effect of encapsulating rejuvenator fiber on the performance of asphalt mixture. Materials, 2019, 12(8): 1266
31. Oliveira L, Lucas J J, Babadopulos L F A L, Soares J B. Stiffness and fatigue evaluation in cyclic tests with rest periods for asphalt mixtures with or without fly ash. Construction and Building Materials, 2022, 322(3): 126426
32. Moharam O, Mostafa A. Improving life cycle of asphalt pavement mixture using Self-Healing Techiuqe. Journal of International Society for Science and Engineering, 2023, 5(3): 63–72
33. Li C, Xiao M, Dong J, Ren J, Guo X. Theoretical and Applied Fracture Mechanics Study on the factors affecting the self-healing performance of asphalt mixture and pavement based on fracture mechanics and calculation formula. Theoretical and Applied Fracture Mechanics, 2023, 126: 103954
34. Bao S, Liu Q, Li H, Zhang L, Maria Barbieri D. Investigation of the release and self-healing properties of calcium alginate capsules in asphalt concrete under cyclic compression loading. Journal of Materials in Civil Engineering, 2020, 33(1): 04020401
35. Tabakovic A, Schlangen E. Self-healing technology for asphalt pavements. Self-healing Materials, 2015: 285–306
36. Inozemtcev S S, Korolev E V. Review of road materials self-healing: problems and perspective. IOP Conference Series. Materials Science and Engineering, 2020, 855(1): 012010
37. Inozemtcev S, Jelagin D, Korolev E, Fadil H, Partl M N, Do T T. Experimental and numerical study on SMA modified with an encapsulated polymeric healing agent. Materials and Structures, 2022, 55(9): 230
38. GOST 31015-2022. Bituminous Stone Mastic Mixtures and Stone Mastic Asphalt. Specifications. Moscow: Gosstroy Rossii, GUP CPP, 2023
39. GOST 12801-98. Materials on the Basis of Organic Binders for Road and Airfield Construction. Test methods. Moscow: Gosstroy Rossii, GUP CPP, 1999
40. Smith M. ABAQUS/Standard User's Manual, 2016
41. Fadil H, Jelagin D, Partl M N. Spherical indentation test for quasi-nondestructive characterization of asphalt concrete. Materials and Structures, 2022, 55(3): 102
42. Maneewongvatana S, Mount D M. Analysis of approximate nearest neighbor searching with clustered point sets. 1999, arXiv: 9901013
43. Virtanen P, Gommers R, Oliphant T E, Haberland M, Reddy T, Cournapeau D, Vázquez-Baeza Y. SciPy 1.0: Fundamental algorithms for scientific computing in Python. Nature Methods, 2020, 17(3): 261–272
44. Thompson A P, Aktulga H M, Berger R, Bolintineanu D S, Brown W M, Crozier P S, Veld P J, Kohlmeyer A, Moore S G, Nguyen T D et al. Plimpton, S. J. LAMMPS—A flexible simulation tool for particle-based materials modeling at the atomic, meso, and continuum scales. Computer Physics Communications, 2022, 271: 108171
45. Wang L. Mechanics of asphalt: Microstructure and micromechanics. International Journal of Pavement Research and Technology, 2012, 5(1): IV–IV
46. Abadeen A Z U, Hussain H, Kumar V S, Murali G, Vatin N I, Riaz H. Comprehensive self-healing evaluation of asphalt concrete containing encapsulated rejuvenator. Materials, 2022, 15(10): 3672
47. Liang B, Lan F, Shi K, Qian G, Liu Z, Zheng J. Review on the self-healing of asphalt materials: Mechanism, affecting factors,

assessments and improvements. Construction and Building Materials, 2020, 266: 120453

48. Gonzalez-Torre I, Norambuena-Contreras J. Recent advances on self-healing of bituminous materials by the action of encapsulated rejuvenators. Construction and Building Materials, 2020, 258: 119568
49. Tang J, Liu Q, Wu S, Ye S, Sun Y, Schlangen E. Investigation of the optimal self-healing temperatures and healing time of asphalt binders. Construction and Building Materials, 2016, 113(8): 1029–1033
50. Concha J L, Norambuena-Contreras J. Thermophysical properties and heating performance of self-healing asphalt mixture with fibres and its application as a solar collector. Applied Thermal Engineering, 2020, 178(5): 115632
51. Pérez I, Gómez-Meijide B, Pasandín A R, García A, Airey G. Enhancement of curing properties of cold in-place recycling asphalt mixtures by induction heating. International Journal of Pavement Engineering, 2021, 22(3): 355–368
52. Wang H, Liu Q, Wu J, Wan P, Zhao F. Self-healing performance of asphalt concrete with ca-alginate capsules under low service temperature conditions. Polymers, 2023, 15(1): 199
53. Yamaç Ö E, Yilmaz M, Yalçın E, Kök B V, Norambuena-Contreras J, Garcia A. Self-healing of asphalt mastic using capsules containing waste oils. Construction and Building Materials, 2020, 270(3): 121417
54. Bhasin A, Palvadi S, Little D. Influence of aging and temperature on intrinsic healing of asphalt binders. Transportation Research Record: Journal of the Transportation Research Board, 2011, 2207(1): 70–78
55. Li Y, Zhang H, Wu Z, Sun B. Influencing factors and evaluation of the self-healing behavior of asphalt binder using molecular dynamics simulation method. Molecules, 2023, 28(6): 2860
56. Chavez-Delgado M, Concha J L, Caro S, Arteaga-Perez L E, Norambuena-Contreras J. Self-healing asphalt with optimised tyre-based pyro-rejuvenator. Fuel, 2025, 400: 135747
57. Li P, Ji R, Zhang C, Xu J, Zheng M, Song X. A study on the road performance of the self-healing microcapsule for asphalt pavement. Materials, 2025, 18(15): 3483